Article:
Szumiata, T., Gzik-Szumiata, M., Brzózka, K. et al. (5 more authors) (2015) Interface influence on the properties of Co90Fe10 films on soft magnetic underlayers - Magnetostrictive and Mössbauer spectrometry studies. Journal of Magnetism and Magnetic Materials, 401. 943 - 948. ISSN 0304-8853

https://doi.org/10.1016/j.jmmm.2015.11.010

Interface influence on the properties of $Co_{90}Fe_{10}$ films on soft magnetic underlayers - magnetostrictive and Mössbauer spectrometry studies

Tadeusz Szumiata*, Małgorzata Gzik-Szumiata, Katarzyna Brzózka,
Bogumił Górka, Michał Gawroński

Department of Physics, Faculty of Mechanical Engineering, University of Technology and Humanities in Radom, 54 Krasickiego Street, 26-600 Radom, Poland
*Corresponding author email: t.szumiata@uthrad.pl

Anastasia Caruana Finkel, Nik Reeves-McLaren, Nicola A. Morley

Department of Materials Science and Engineering, University of Sheffield, Mappin Street, Sheffield S1 3JD, UK

A B S T R A C T

The main aim of the work was to show the correlation between magnetostrictive properties and microstructure of 25 nm thick $Co_{90}Fe_{10}$ films deposited on soft magnetic underlayers. A special attention was paid to the role of the interface region. In the case of $Co_{90}Fe_{10}$ on 25 nm and 35 nm thick METGLAS underlayers one can resolve in conversion electron Mössbauer spectra two hyperfine field distributions (high-field and medium-field ones) corresponding to both constituents of bilayers. Analogical distributions describe the spectra of $Co_{90}Fe_{10}$ on 25 nm and 35 nm thick $Ni_{81}Fe_{19}$ underlayers, however an additional low-field, smeared component has been observed. It has been attributed to the interface layer (of partially disordered structure) between magnetostrictive layer and soft magnetic layer. Such interpretation is backed up by the obtained strong correlation between mean hyperfine field value and magnetostriction constant of the films. The investigated bilayers are good candidates for MRAM devices.

Keywords: low-magnetostrictive thin films; interface effects; Mössbauer spectrometry

1. Introduction

Thin soft magnetic $Co_{90}Fe_{10}$ films are found in a range of applications including high-density recording heads, magnetic random access memory (MRAM) and magnetic sensors [1,2]. This is because they have high saturation magnetisation (>1500 kAm^{-1}), accompanied by good soft magnetic properties, such as coercive fields less than 2.5kAm^{-1} and magnetostriction constants less than 10 ppm [3, 4]. Often these films are grown on underlayers, which can change the texture, stress and grain size of the film along with the magnetic properties, i.e. decrease the coercive field (H_c) and increase the magnetostriction constant (λ_s) [5,6]. It is therefore important to understand how these magnetic properties vary with different underlayers, to ensure that they are not going to have an adverse effect on the application they are being used in. It is also important to thoroughly investigate the interface in order to understand how it influences the change in the magnetic properties.

Cakmaktepe et al [5], studied the effect of thin underlayers of Cu, Cr, Au and NiFe on the structural and magnetic properties of 40nm $Co_{90}Fe_{10}$ films. They found that all the underlayers reduced the coercive field of the $Co_{90}Fe_{10}$ films, with Au inducing the strongest uniaxial anisotropy present. The reduction they concluded was due to the $Co_{90}Fe_{10}$ being single domain on the underlayer, rather than multi-domain when grown without an

underlayer. They also determined that the underlayers changed the texture within the films, from (110) to (200) when grown on Au underlayers and (220) when grown on Cu underlayers. Cai et al [7] investigated the structural and magnetic properties of 100nm $Co_{90}Fe_{10}$ films on Cu, NiFe and Zr underlayers, which included annealing the samples after growth. They found that the Cu and NiFe underlayers did not affect the texture present in the $Co_{90}Fe_{10}$ films with the films containing both fcc(111) and hcp(100) texture. While the $Co_{90}Fe_{10}$ films were grown on Zr, the films only had fcc(111) texture. The magnetic properties of the $Co_{90}Fe_{10}$ films did not change when deposited on the Cu and NiFe underlayers, nor annealing the films did affect the magnetic properties of these bilayers. For the $Co_{90}Fe_{10}$ films on Zr, annealing the films increased the grain size in the $Co_{90}Fe_{10}$ films, along with decreasing the coercive field. Thus Zr strongly influenced the texture and magnetic properties of $Co_{90}Fe_{10}$ films. Piramanayagam et al [8] studied the effect of Ta and Pd underlayers on 40nm $Co_{90}Fe_{10}$ films. They found that growing on Ta reduced the coercive field by a factor 5, due to a change in texture of the films. Fernandez-Outon et al [9] investigated the interface between IrMn and CoFe to determine how the sharpness of the interface changed with annealing and how this change the coercive field and the exchange field. They used conversion electron Mössbauer spectroscopy to determine the magnetic hyperfine fields and how they related to the interface and magnetic properties. Fukuzawa et al [4] investigated how the magnetostriction constant of 2nm $Co_{90}Fe_{10}$ films changed for Ru and Cu underlayers. They found that the magnetostriction constant could be positive or negative depending on which underlayer it was grown on. Also the magnetostriction constant varied as a function of the underlayer thickness.

Previous work by Caruana Finkel et al [6] showed that the magnetostriction constant of the $Co_{90}Fe_{10}$ films strongly depended on the underlayer they were grown on. For Metglas underlayers the effective magnetostriction constant was ~15ppm, independent of underlayer thickness, while for the NiFe underlayer the magnetostrictive constant was positive for the 15nm NiFe/25nm CoFe film but negative for the 35nm NiFe/25nm CoFe. This paper takes this research further to determine the reason behind the change from positive to negative magnetostriction constants in these bilayers, by using Mössbauer spectrometry to study the hyperfine magnetic fields and to determine the role of the interface.

2. Experimental Set-up

The bilayer films studied were all grown on silicon substrates with the native oxide layer still in place. The silicon was washed with acetone followed by isopropanol to remove any residue on the surface, before being placed in the sputterer. The bilayers were all grown in a Nordiko NM2000 RF sputterer, which had the capability to grow both layers without exposing the films to air, during the growth. The targets used for the films growth were $Ni_{81}Fe_{19}$ (NiFe, permalloy), METGLAS ® 2605SC of $Fe_{81}B_{13.5}Si_{3.5}C_2$ (Metglas) and $Co_{90}Fe_{10}$ (CoFe). The NiFe and Metglas layers were grown at 4.5 mTorr with power densities of 1 kWm^{-2} and 1.5 kWm^{-2} respectively. The CoFe layer was grown at 4.8 mTorr and at a power density of 2 kWm^{-2}. The Ar growth pressures were chosen to ensure uniform growth of the films, along with being the lowest stable pressure of the system, which is important for NiFe films [10]. The power densities were chosen as they gave good control of the thickness of each of the layers. The series of bilayers were grown with no applied magnetic field. The underlayer thickness ranged from 15 nm to 35 nm, with the CoFe film thickness always being 25nm. Schematic drawing of the films and the photo of the real sample is presented in Fig. 1.

The magnetic hysteresis loops of all the bilayers were measured using a magneto-optic Kerr effect (MOKE) magnetometer [6]. From the normalised hysteresis loops, the coercive field (H_c), anisotropy field (H_k) and remanent magnetisation (M_R) were determined. For each

film, a series of hysteresis loops were measured as a function of the angle between the in-plain field direction and the long axis of the film - this allowed the anisotropy to be inferred [6]. The effective magnetostriction constant (λ_{eff}) of each film was determined using the Villari Effect [11]. The technique used involved bending the film over a series of known bend radii, and measuring the magnetisation hysteresis loop for each radius on a MOKE magnetometer. From the magnetisation loop, the anisotropy field is determined and then plotted against the inverse bend radii (R). The effective magnetostriction constant is then calculated using [11]:

$$\lambda_{\text{eff}} = \frac{d(H_{\text{k}})}{d\left(\frac{1}{R}\right)} \frac{2\mu_0 M_{\text{s}}(1-\upsilon^2)}{3\tau E}$$

where $\mu_0 M_s$ is the saturation magnetisation, υ is the Poisson ratio of the substrate (for silicon: 0.28), E is the Young's Modulus of the substrate (silicon: 130GPa) and τ is the substrate thickness (silicon: 500 ± 50 μm).

Conversion electron Mössbauer spectroscopy (CEMS) was utilised at room temperature in order to study the structural and magnetic order as well as phase content of the thin $Co_{90}Fe_{10}$ films on different underlayers. The system consisted of ^{57}Co(Rh) X-ray source on a vibrator moving with constant acceleration, and gas flow type conversion electron detector (Model MM/CED-3) in 2π backscattering mode for counting the resonant 7.3 and 5.6 keV electrons (generated by the internal conversion process). The same equipment was successfully applied for the recent investigations of high-magnetostrictive Fa-Ga thin layers [12-14]. The thickness both of previous and present samples was smaller than penetration depth of conversion electrons [15] thus our thin layered structures were probed over the full cross-section. In order to obtained sufficient statistics each spectrum had to be collected more than one week.

For the fitting of CEMS spectra Voigt-type profiles were used, which represent a convolution of Zeeman sextets (six Lorentzian lines) with Gaussian hyperfine field distributions. Such approach is very common in the case of the disordered alloys. A numerical minimisation of $\chi 2$ function was performed by means of PolMoss software (based on MS Excel Solver extension) offering both gradient and evolutionary algorithms. Previously, this package was effectively applied for CEMS spectra analysis of in the case of Fa-Ga thin layers [12-14].

3. Results and discussion

Figure 2 presents room temperature CEMS spectra of four 25 nm thick $Co_{90}Fe_{10}$ films on Metglas ($Fe_{81}B_{13.5}Si_{3.5}C_2$) and Permalloy ($Ni_{81}Fe_{19}$) underlayers. In the case of the $Co_{90}Fe_{10}$ on Metglas 25nm and 35 nm thick underlayers (Fig. 2a and Fig. 2b, respectively) the Mössbauer spectra were fitted with two components as quasi-continuous hyperfine field distributions. The high-field component was attributed to $Co_{90}Fe_{10}$ alloy on top layer, whereas the low-field one - to the Metglas alloy, which constitutes the underlayer. The corresponding hyperfine field distributions (HFD) are plotted in Fig. 3a and Fig. 3b. The hyperfine parameters values and the contributions of each component are listed in Table 1. As reported in previous paper [6] all investigated $Co_{90}Fe_{10}$ layers have fcc structure what is typical for bulk alloy of similar atomic content and was confirmed in literature for electrodeposited micrometer layers on graphite [16,17]. The mean values of hyperfine field distribution for both $Co_{90}Fe_{10}$ layers on Metglas were $\langle B_{hf} \rangle \approx 32$ T, which are very similar to those of corresponding films investigated by Jartych et al [16,17], which were 31.9 T – 32.5 T. In the

case of simple $Co_{90}Fe_{10}$ alloy the Mössbauer spectra are usually reproduced by a discrete set of Zeeman sextets corresponding to the different atomic surroundings of iron (different numbers of Fe and Co atoms in the first and the second coordination zone). In our case due to the complexity and not perfect statistics of CEMS spectra the applications of HFD was the only reasonable solution. A halfwidth (standard deviation) of HFD part attributed to $Co_{90}Fe_{10}$ is about twice bigger than determined in [16] which can be both a sign of greater structural inhomogeneity and a result of possible stress distribution inside the layer. The obtained isomer shift ~ 0.05 mm/s (IS – relative to pure iron) was bigger than value referenced in [16] (< 0.01 mm/s), which could also point to the internal stress. Quadrupole splitting (QS) mean values are negligibly small, which is typical either for not deformed cubic structure or for partially amorphous system in magnetic state. The values of hyperfine field parameters – especially mean hyperfine field – reported in literature [16-20] have quite significant spread (29.8 T – 33.2 T) – depending on the samples form (thin layers, particles) and size (thickness). However, in our case there is no noticeable difference between the parameters for $Co_{90}Fe_{10}$ film on 25 nm and 35 nm Metglas underlayer. Moreover, in both cases mean hyperfine field of the component corresponding to Metglas is of the order of 21.5 T, whereas references concerning Metglas 2605SC [21-23] and other kinds of Metglas alloys [25-28] report significantly higher values – from 23 T even to 29 T (typically about 25 T). The possible reason of this discrepancy is that above specified references relate to the Metglas in the form of melt-spun ribbons of submillimetre thickness (i.e. almost bulk system), whereas we investigated nano-underlayers of Metglas. Small thickness, influence of Si substrate and interface regions as well as internal stress can modify the magnetic and hyperfine interactions in thin Metglas film. Such effect of the reduction of hyperfine field in laser ablated thin films of Metglas 2605SC (to about 22.3 T) is described in [24] – both mean value of hyperfine field and halfwidth of HFD are quite close to the data obtained for the CoFe/Metglas films in this paper. Dispersion values of Metglas HFD are about four times bigger than for Fe-Co layer, which clearly illustrates a difference in structure of the amorphous and partially disordered solid alloys. In the hyperfine field distributions of our Metglas underlayers one can find a small, low-field tail, that could point to the structural inhomogeneity (possibly in the Fe-Co/Metglas interface region or close to the silicon substrate). Such interpretation is justified by the fact that presence of such tail is not supported in the Mössbauer spectra for the quasi-bulk amorphous METGLAS ® 2605SC ribbons [26]. In practice in the reported HFD distributions there are two neighbouring low-field peaks – positive one and negative one – but almost averaging out to zero, which is a fingerprint of numerical artefact. The isomer shift values listed in Table 1 are consistent (within experimental error) with reference data for Metglas [21-28], as well as quadrupole splitting values – relatively small ones – pointing to the almost cubic symmetry of local environments of Fe atoms in the amorphous alloy. The contributions of components in transmission Mössbauer spectra are directly related to the relative amount of iron present in given phase or subsystem. In the case of CEMS experiment there is no such simple correspondence due to the fact that conversion electrons are emitted from regions of different depth [15], which strongly influences the detection efficiency. The P-values listed in Table 1 only qualitatively show that iron content in Fe-Co layer is several times lower than that in Metglas underlayer and a slight increase of Metglas contribution in the second sample well correlates with greater thickness of the underlayer.

The Mössbauer spectra of 25 nm thick $Co_{90}Fe_{10}$ films on 25 nm and 35 nm thick Permalloy ($Ni_{81}Fe_{19}$) underlayers (Fig. 2c and 2d, respectively) were analysed using three quasi-continuous hyperfine field distributions (Fig. 3c and 3d). High field component – as in previous case – corresponds to the $Co_{90}Fe_{10}$ alloy. The values of all hyperfine parameters describing this subspectrum are very similar to those for the $Co_{90}Fe_{10}$ films on Metglas underlayers (Tab. 1), however the mean hyperfine field is slightly lower. This could suggest a

possible dependence of internal stress in $Co_{90}Fe_{10}$ films on the kind of underlayer. The second component in CEMS spectra is attributed to the fcc-structured $Ni_{81}Fe_{19}$ Permalloy layer. The obtained mean values of HFD (23.4 – 25.2 T) are significantly lower than expected for this kind of disordered alloy (around 30 T [17,29]), however the results of reported in [30,31] investigations of nanometer-thick Permalloy films of nanocrystaline structure also demonstrate a considerable reduction of mean hyperfine field (to about 27 T). In our case this reduction is even more pronounced not only because of nanometer thickness of Permalloy layers but also due to the influence both of substrate and top $Co_{90}Fe_{10}$ layer as well as the interface region. The shape and dispersion $\Delta(B_{hf})$ of HFD as well as small values of quadrupole splitting QS are consistent with reported data [29,30], whereas isomer shift IS is higher than for thick Permalloy layers [17]. Both isomer shift and mean hyperfine field value discrepancies clearly point to the strong internal stress and possible structural deformations in the Permalloy layers. The third low-field component in the Mössbauer spectra has been assigned to the interface region. Its contribution in $Co_{90}Fe_{10}$ film on 25 nm thick Permalloy layer is almost 22%, whereas in the case of 35 nm Permalloy underlayer this component dominates (60%), which could be a result of the strong interdiffusion between $Co_{90}Fe_{10}$ and $Ni_{81}Fe_{19}$ layers. Thus, the elemental content of interface corresponds to the Co-Ni-Fe ternary alloy. The magnetic phase diagram of such alloy (measured by means of Mössbauer spectrometry and polarised neutron diffraction [32]) is very complex and exhibits the instabilities of the ferromagnetic ordering for some ranges of atomic concentrations. Moreover, even intentionally deposited Co-Ni-Fe films are multiphase systems (as mixture both of binary and ternary phases of bcc, fcc and hcp crystalline structures [33]). These facts explain the observed wide spread of HFD for the interface region, as well as weakening of magnetic spin-spin interactions (seen as a low value of mean hyperfine field – smaller than 6 T). The relative contributions of all the subspectra show that in the case of the sample on thicker underlayer the interface region is constituted predominately with Permalloy, however the absolute contribution of $Co_{90}Fe_{10}$ to the interface is still 2 times greater than in the case of thinner underlayer. Another fingerprints of the structural inhomogeneity of the interface region are the high values of isomer shifts (IS > 0.5 mm/s, Tab. 1). Quadrupole splittings QS have been just fixed to zero, in order to limit the number of fitting parameters in the spectra of not perfect statistics. The higher contribution of interface region in the case of the sample with thicker underlayer (35 nm) – outwardly astonishing – could point to the fact, that in this film the process of interdiffusion was more intense e.g. due to the different distribution of the internal stress. The best fits of the CEMS spectra for all samples $Co_{90}Fe_{10}$ (both on Metglas and Permalloy underlayers) were obtained when in all Zeeman sextets the ratio of the second and the fifth lines intensities to the third and fourth ones was equal to 4. It points to the in-plane alignment of the spins for all magnetic phases as a result of the strong shape magnetic anisotropy in the investigated thin films.

The interpretation of the third component in the CEMS spectra as $Co_{90}Fe_{10}/Ni_{81}Fe_{19}$ interface region demands a critical evidence and further arguments. The presence of the additional subspectra frequently point to the degradation of the top part of the thin-layered structure as a result of the oxidation (corrosion) process. However, one can reject such option, because as mentioned in “Experimental Set-up” section, the Nordiko NM2000 RF sputterer had the feature to grow layers without exposing the films to air in order to avoid the oxidation. Moreover it is worth underling that the second set of samples, grown with applied magnetic field, was investigated in [6] – mainly their structural and magnetic properties where studied in details. There was no significant difference between result for both sets of the samples – thus, the fabrication process of the samples seemed to be repeatable and providing the protection of the samples against oxidation. Without such conclusion one could claim that the central parts of the CEMS spectra for $Co_{90}Fe_{10}/Ni_{81}Fe_{19}$ samples contain the paramagnetic

doublet of parameters close to those for wustite iron oxide (FeO), however even in such case the doublet itself (without low-value HFD) would be not sufficient in order to reproduce well the centre of the spectra. The complicated shape of HFD attributed to the interface region presumably originates from the – already mentioned – complexity of phase diagram for Co-Ni-Fe ternary alloy [32].

The important indication for this discussion could be the fact that previous article [6] reports a dramatic change of magnetostriction constant of the samples on 35 nm thick Permalloy underlayers. In this case a saturation magnetostriction constant (determined by means of the Villari Effect methods) even changes its sign. One possible reason could be a structural phase transition or/and the change of crystalline texture of $Co_{90}Fe_{10}$ magnetostrictive layer, however it is not supported by x-ray data [6]. Moreover, it is clearly visible in Tab. 1, that the increasing contribution of the third component is accompanied by the contribution decrease of both previous components. Thus it means that a new phase is formed between $Co_{90}Fe_{10}$ and $Ni_{81}Fe_{19}$ layers and it can be qualified as interface region. The strong influence of the surface effects, roughness and interfaces on the effective magnetostriction of thin films and MagMEMS devices is well known feature both from experimental and theoretical point of view [34]. Thus the correlation between the saturation magnetostriction constant of the all samples and mean hyperfine field of $Co_{90}Fe_{10}$ layers together with interface regions were studied. The justification for such analysis was the fact that effective magnetostriction constant depends not only on relative amounts of the magnetostrictive phases, but is also sensitive to the possible changes of magnetic interactions within phases. The results plotted in Fig. 4 demonstrate a monotonic (almost linear) trend, which means that interface region noticeably influences the effective magnetostriction constant of the bilayer films.

4. Conclusions

The conversion electron Mössbauer spectrometry together with magnetostriction measurements has appeared to be an effective tool for $Co_{90}Fe_{10}$ thin films characterization – complementary to the standard x-ray diffraction and magnetometry [6]. The detailed analysis of hyperfine parameters allowed to gain additional information about the structure and magnetism of $Co_{90}Fe_{10}$ thin layers sputtered on the different underlayers. In particular, the clear signs of internal stress and structural inhomogeneity were found in the investigated layers. Two samples on Metglass underlayer of different thickness were characterised by similar hyperfine field distribution of all system and by similar effective magnetostriction constant. In the case of samples deposited on Permalloy buffer a significant change in magnetostriction constant was observed from positive to negative one (along with underlayer thickness alteration), which was strongly correlated with decrease of mean hyperfine field. This trend as well as presence of additional component in CEMS spectra support the interpretation which assigns the observed phenomena to the influence of the interface region. The role of this interlayer zone can be crucial in tailoring the magnetoelastic properties of the future MRAM and MagMEMS devices.

Acknowledgements

This work was supported, in part, by Polish Ministry of Science and Higher Education under statutory funds granted to the Department of Physics in the University of Technology and Humanities in Radom for 2015 year.

References

[1] M. Mao, T. Schneider, R. Bubber, J. Kools, X. Liu, Z Aaltounian, C.-L. Lee, A. Devasahayam and K. Rook, Optimization of high B_{sat} FeCo films for write pole applications, Journal of Applied Physics, 97 (2005) 10F908.

[2] H. Yoda, H. Iwasaki, T. Kobayashi, A. Tsutai and M. Sahashi, Dual-element GMR/Inductive heads for Gigabits density recording using CoFe spin-valves, IEEE Transaction on Magnetics 32 (1996) 3363–3367.

[3] E. J. Yun, W. Win and R. M. Wasler, Magnetic properties of RF diode sputtered Co_xFe_{1-x} alloy thin films, IEEE Transactions on Magnetics 52 (1996) 4535– 4537.

[4] H. Fukuzawa, Y. Kamiguchi, K. Koi, H. Iwasaki and M. Sahashi, Saturation magnetostriction of an ultrathin CoFe free-layer on double-layered underlayers, Journal of Applied Physics 91 (2002) 3120–3124.

[5] S. Cakmaktepe, M. I. Coskun and A. Yildiz, Underlayer effect of structural and magnetic properties of $Co_{90}Fe_{10}$ thin films, Lithuanian Journal of Physics 53 (2013) 112–117.

[6] A. Caruana Finkel, N. Reeves-McLaren and N. A. Morley, Influence of soft magnetic underlayers on magnetic properties of Co90Fe10 films, Journal of Magnetism and Magnetic Materials 357 (2014) 87–92.

[7] J.-W. Cai, O. Kitakami and Y. Shimada, The effects of buffer layers on the crystalline structures and magnetic properties of Co-rich and Co-Fe and Co-Fe-Al films, J. Phys. D: Appl. Phys. 28 (1995) 1778–1784.

[8] S. N. Piramanayagam, M. J. Liau, J. Z. Shi and B. C. Lin, Textured growth CoFe for soft underlayers in CoCrPt:SiO_2 perpendicular magnetic recording media, Journal of Magnetism and Magnetic Materials 303 (2006) e152–e155.

[9] L. E. Fernandez-Outon, M. S. Araujo Filho, R. E. Araujo, J. D. Ardisson and W. A. A. Macedo, Setting temperature effect in polycrystalline exchange-biased IrMn/CoFe bilayers, Journal of Applied Physics 113 (2013) 17D704.

[10] A. V. Svalov, I. R. Aseguinolaza, A. Garcia-Arribas, I. Orue, J. M. Barandiaran, J. Alonso, M. L. Fenandez-Gubieda and G. V. Kurlyandskaya Structure and Magnetic properties of Thin permalloy films near the “Transcritical” state, IEEE Trans. Mag. 46 (2010) 333–336.

[11] A. Javed, N. A. Morley and M. R. J. Gibbs, Structure, magnetic and magnetostrictive properties of as-deposited Fe-Ga thin films, Journal of Magnetism and Magnetic Materials 321 (2009) 2887–2882.

[12] A. Javed, T. Szumiata, N. A. Morley, M. R. J. Gibbs, An investigation of the effect of structural order on magnetostriction and magnetic behavior of Fe–Ga alloy thin films, Acta Materialia 58 (2010) 4003–4011.

[13] A. Javed, N. A. Morley, T. Szumiata, M. R. J. Gibbs, A comparative study of the microstructural and magnetic properties of <110> textured thin polycrystalline $Fe_{100-x}Ga_x$ ($10 \leq x \leq 35$) films, Applied Surface Science 257 (2011) 5977–5983.

[14] T. Szumiata, K. Brzózka, M. Gawroński, B. Górka, A. Javed, N. A. Morley and M. R. J. Gibbs, Structural and magnetic ordering in Fe-Ga thin films examined by Mössbauer spectrometry, Acta Physica Polonica A 119 (2011) 21–23.

[15] M. Seberíni, J. Sitek, Surface analysis of iron–containing samples by CEMS and overview of the method, Journal of Electrical Engineering 59 (2008) 234–240.

[16] E. Jartych, J. K. Żurawicz and M. Budzyński, A Mössbauer study of electrodeposited $Fe_{1-x}Co_x$ alloys, J. Phys.: Condens. Matter 5 (1993) 927–934.

[17] E. Jartych, J. K. Żurawicz and M. Budzyński, Mössbauer investigation of electrodeposited Fe-Ni, Fe-Co and Co-Ni:^{57}Fe alloys, Nukleonika 39 (1994) 215–222.

[18] R. A. Brand, O. Bohné, W. Keune, Mössbauer studies of magnetic anisotropy in $Pt/Fe_{1-x}Co_x$ multilayers, Journal of Magnetism and Magnetic Materials 104–107 (1992) 1891–1892.
[19] R.A. Brand, Th. von Schwartzenberg, O. Bohné, W. Keune, Local magnetic properties of $Pt/Fe_{1-x}Co_x$ multilayers studied by Mössbauer spectroscopy, Journal of Magnetism and Magnetic Materials 126 (1993) 248–250.
[20] Yu. I. Petrov and E. A. Shafranovskii, Specific features of the hyperfine field at iron nuclei in aerosol nanoparticles of FeCo alloy, Doklady Physical Chemistry 440 (2011) 178–182.
[21] N. Saegusa and A. H. Morrish, Mössbauer study of amorphous $Fe_{81}B_{13.5}Si_{3.5}C_2$, Phys. Rev. B26 (1982) 10–15.
[22] N. Saegusa and A. H. Morrish, Surface atomic rearrangements and crystalline transformations in amorphous $Fe_{81}B_{13.5}Si_{3.5}C_2$ ribbons, Phys. Rev. B26 (1982) 6547–6553.
[23] A. K. Bhatnagar, B.B. Prasad and R. Jagannathan, Study of magnetic and hyperfine interactions in the quaternary amorphous alloy $Fe_{81}B_{13.5}Si_{3.5}C_2$, Phys. Rev. B29 (1984) 4896–
[24] I. Bibicu, Mössbauer spectroscopy applied to surfaces and interfaces, Rom. Journ. Phys. 49 (2004) 893–900.
[25] J. M. Cadogan, S. J. Campbell, J. Jing, C. P. Foley, P. Kater, Y. W. Mai, Annealing embrittlement of $Fe_{78}Si_9B_{13}$ (METGLAS-2605S2), Hyperfine Interactions 226 (2014) 7–14.
[26] T. Nagarajan, U. Chindambaram Asari, S. Srinivasan, V. Sridharan and A. Narayanasamy, Amorphous phase separation in METGLAS 2605CO, Hyperfine Interactions 34 (1987) 491–494.
[27] I. Vincze, Evaluation of complex Mössbauer spectra in amorphous and crystalline ferromagnets, Solid State Communications 25 (1978) 689–693.
[28] A. López-Morales, A. Cabral-Prieto, F. García-Santibáñez, J. Ramírez, J. López-Monroy, Micro-structural changes in the amorphous Fe-based alloy 2605S3A prior to crystallization, Internet Electronic Journal Nanociencia et Moletrónica 8 (2010) 1445–1458.
[29] E. Jartych, M. Budzyński, J. K. Żurawicz, Hyperfine interactions in electrodeposited Fe_xNi_{1-x} alloys, Hyperfine Interactions 73 (1992) 255–264.
[30] P. Prieto, J. Camarero, J. F. Marco, E. Jiménez, J. M. Benayas, and J. M. Sanz, Characterization of nanocrystalline permalloy thin films obtained by nitrogen IBAD, IEEE Transactions on Magnetics 44 (2008) 3913–3916.
[31] P. Auric, S. Bonat, and B. Rodmaq, Structural and magnetic properties of annealed $[Fe_{19}Ni_{81}]_{12Å}/Ag_{11Å}$ multilayers studied by Mössbauer spectroscopy, x-ray diffraction and magnetization measurements, J. Phys: Condens. Mater. 10 (1998) 3755–3768.
[32] N. Kunitomi, Y. Nakai, K. Yamasaki, N. Schibuya, Atomic magnetic moment in ternary alloy Fe-Co-Ni, Journal de Physique Colloques 35 (1974) C4-149–C4-151.
[33] Daheum Kim, D.-Y. Park, B. Y. Yoo, P. T. A. Sumodjo, N. V. Myung, Magnetic properties of nanocrystalline iron group thin film alloys electrodeposited from sulfate and chloride baths, Electrochimica Acta 48 (2003) 819–830.
[34] T. Szumiata, M. Gzik-Szumiata, Surface Magnetostriction Model for MagNEMS, Acta Physica Polonica A 126 (2014) 200–201.

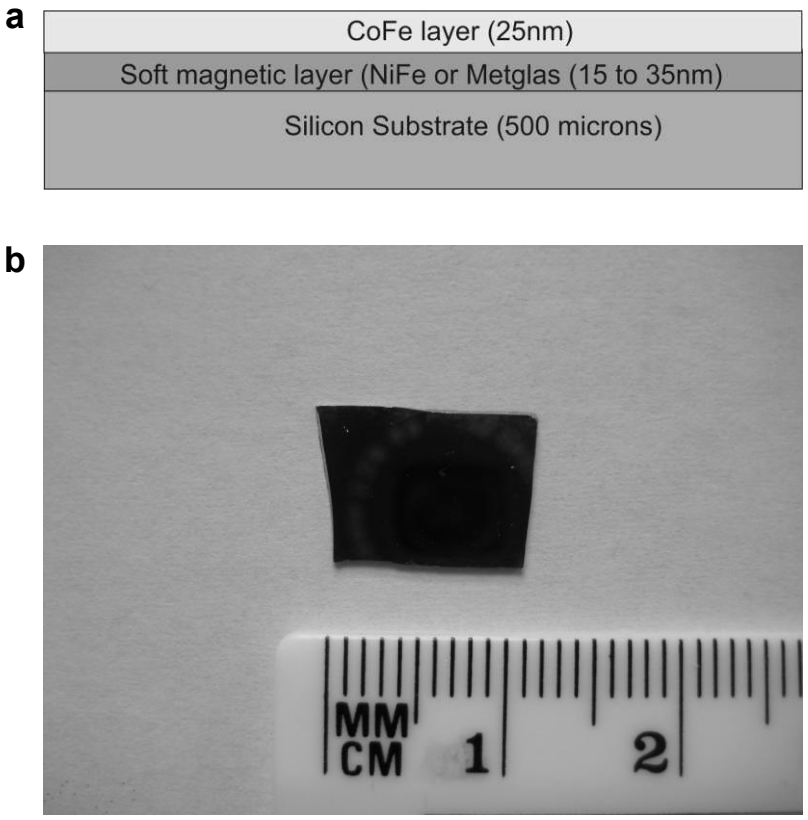

Fig. 1. a) Schematic drawing of the bilayered films. b) Photo of the real sample.

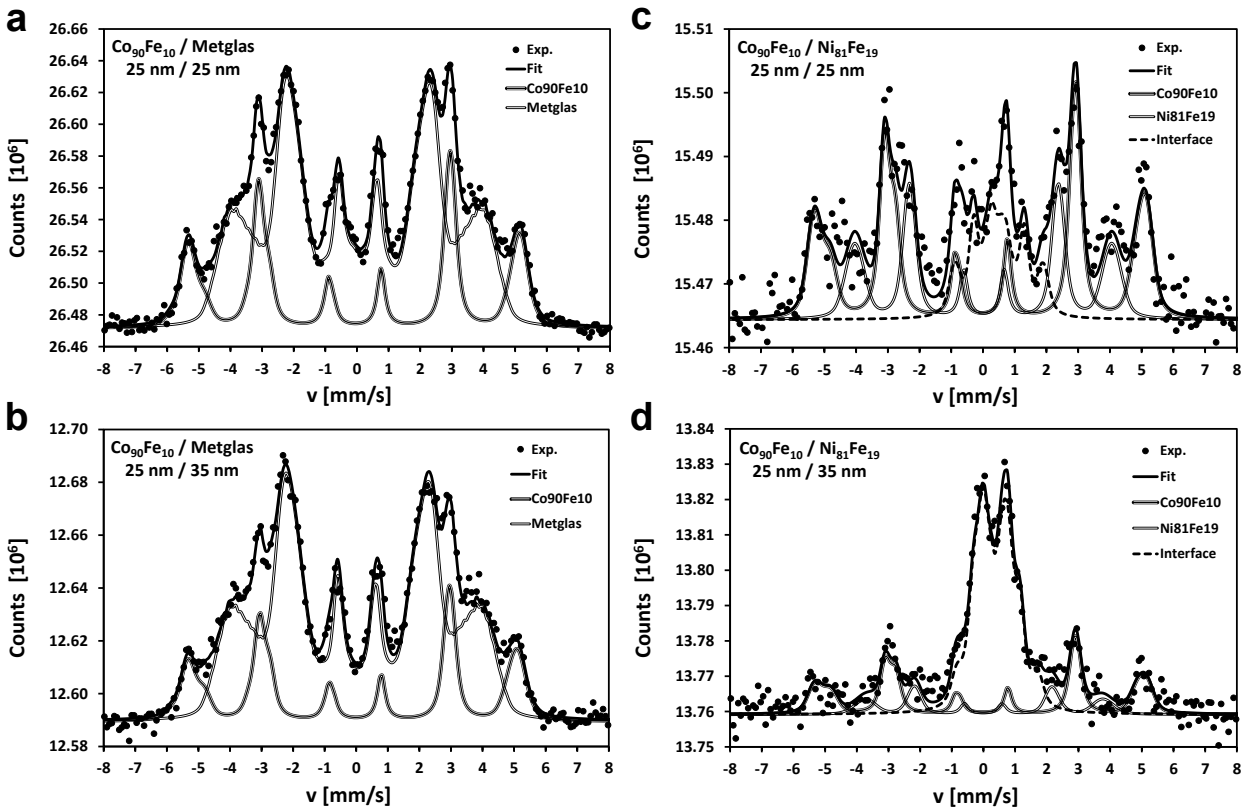

Fig. 2. CEMS spectra at room temperature for 25 nm $Co_{90}Fe_{10}$ layers on a) 25 nm Metglas, b) 35 nm Metglas, c) 25 nm $Ni_{81}Fe_{19}$ and d) 35 nm $Ni_{81}Fe_{19}$ underlayers.

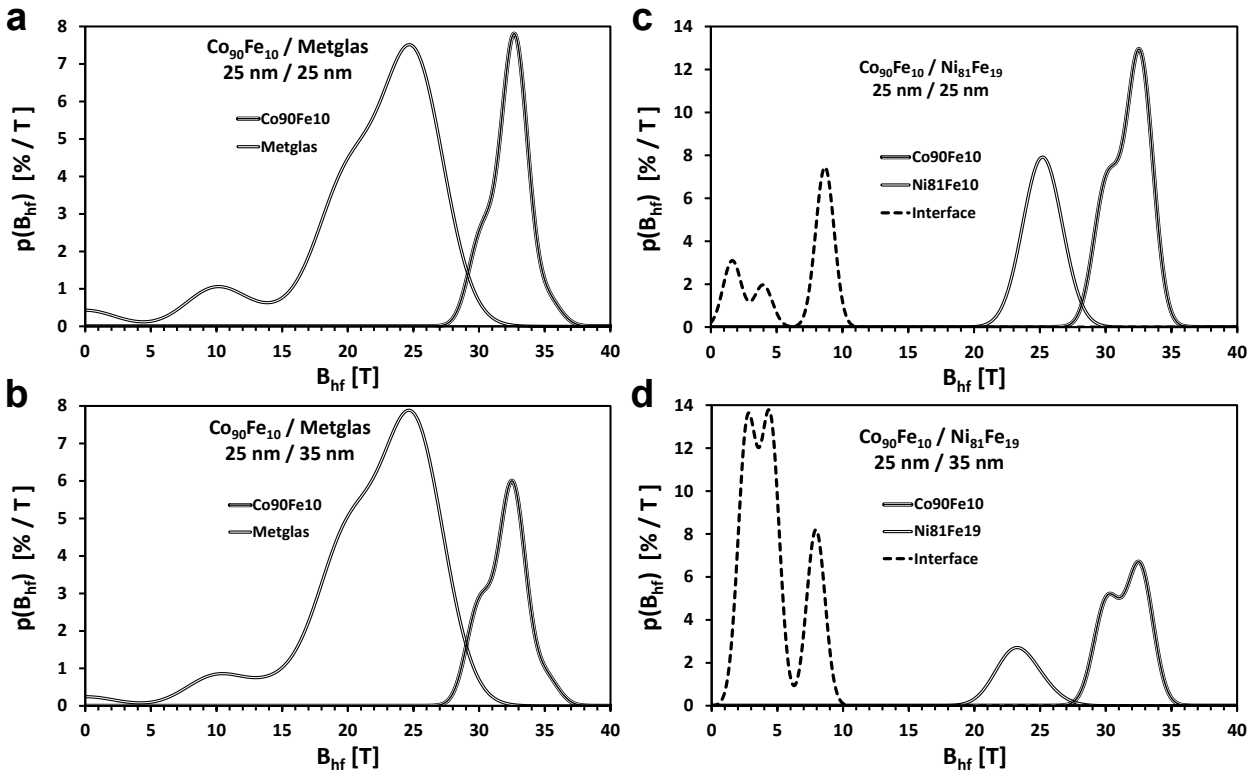

Fig. 3. Hyperfine field distributions at room temperature for 25nm $Co_{90}Fe_{10}$ layers on a) 25 nm Metglas, b) 35 nm Metglas, c) 25 nm $Ni_{81}Fe_{19}$ and d) 35 nm $Ni_{81}Fe_{19}$ underlayers.

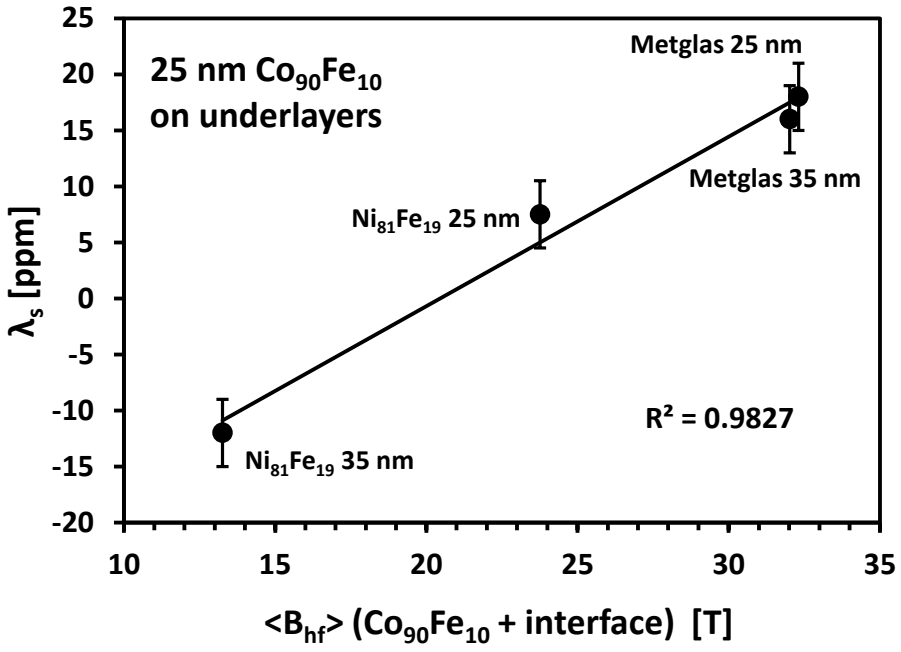

Fig. 4. Correlations of saturation magnetostriction constant with mean hyperfine field of $Co_{90}Fe_{10}$ layers and interface regions on different underlayers.

Table 1. Parameters of CEMS spectra and corresponding hyperfine field distributions for $Co_{90}Fe_{10}$ films on different underlayers ($<B_{hf}>$ - mean hyperfine field, $\Delta(B_{hf})$ – halfwidth of hyperfine field distribution (dispersion), <IS> - mean isomer shift (relatively to Fe foil), <QS> - mean quadrupole splitting, P – contributions of the components

Film	Component	$<B_{hf}>$ [T]	$\Delta(B_{hf})$ [T]	<IS> [mm/s]	<QS> [mm/s]	P [%]
25 nm $Co_{90}Fe_{10}$ on 25 nm Metglas	$Co_{90}Fe_{10}$	32.3	2.3	0.05	-0.01	27.0
	Metglas	21.2	8.2	0.13	0.03	73.0
25 nm $Co_{90}Fe_{10}$ on 35 nm Metglas	$Co_{90}Fe_{10}$	32.0	2.4	0.06	-0.06	23.3
	Metglas	21.6	7.4	0.11	-0.01	76.7
25 nm $Co_{90}Fe_{10}$ on 25 nm $Ni_{81}Fe_{19}$	$Co_{90}Fe_{10}$	31.7	2.2	0.07	-0.01	48.3
	$Ni_{81}Fe_{19}$	25.2	1.5	0.13	-0.02	29.8
	Interface	6.2	3.8	0.58	0.00	21.9
25 nm $Co_{90}Fe_{10}$ on 35 nm $Ni_{81}Fe_{19}$	$Co_{90}Fe_{10}$	31.5	2.2	0.07	-0.02	28.4
	$Ni_{81}Fe_{19}$	23.4	2.3	0.12	0.03	11.6
	Interface	4.6	2.7	0.48	0.00	60.0

Figure

Click here to download high resolution image

Figure

Click here to download high resolution image

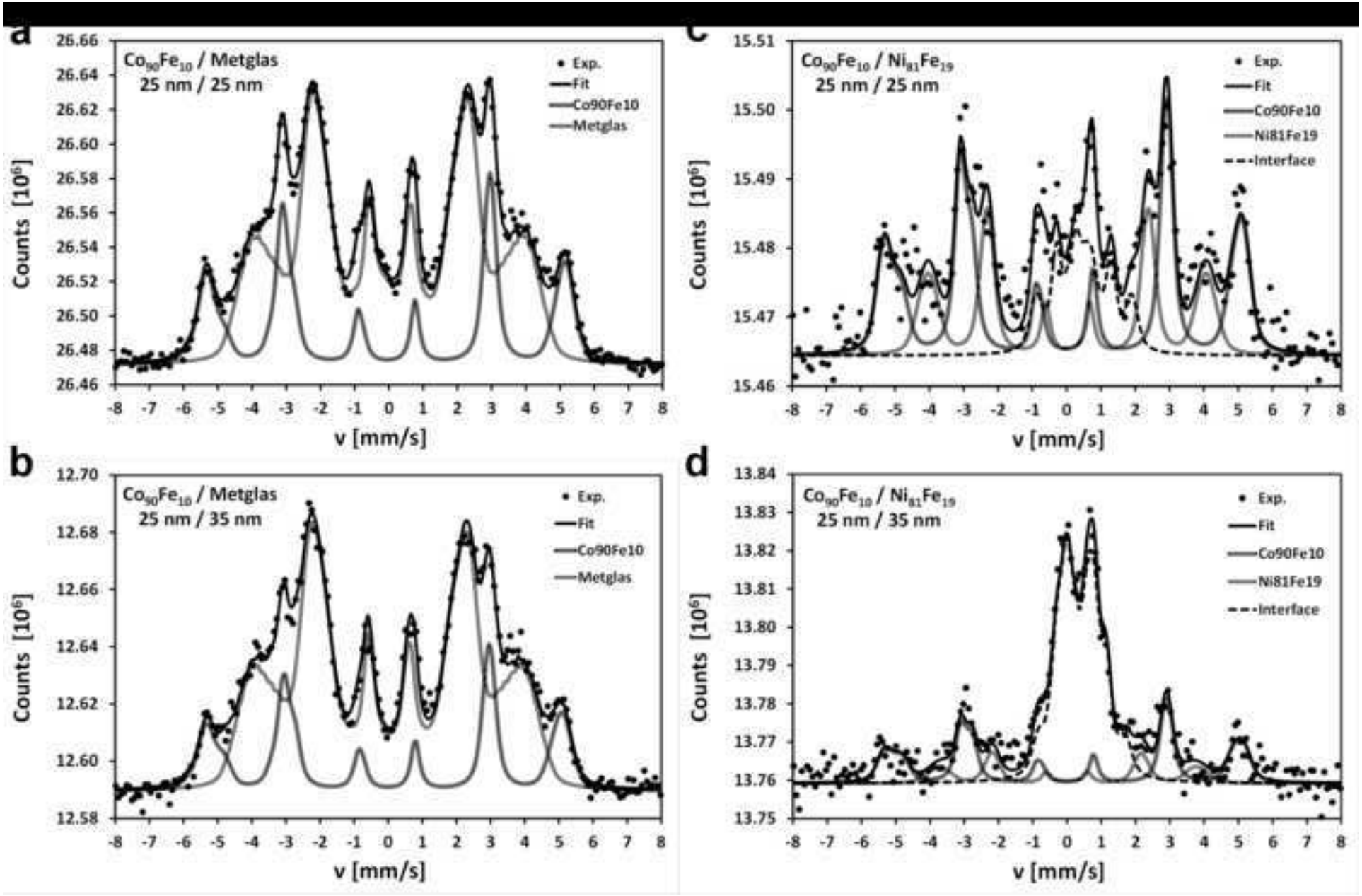

Figure

Click here to download high resolution image

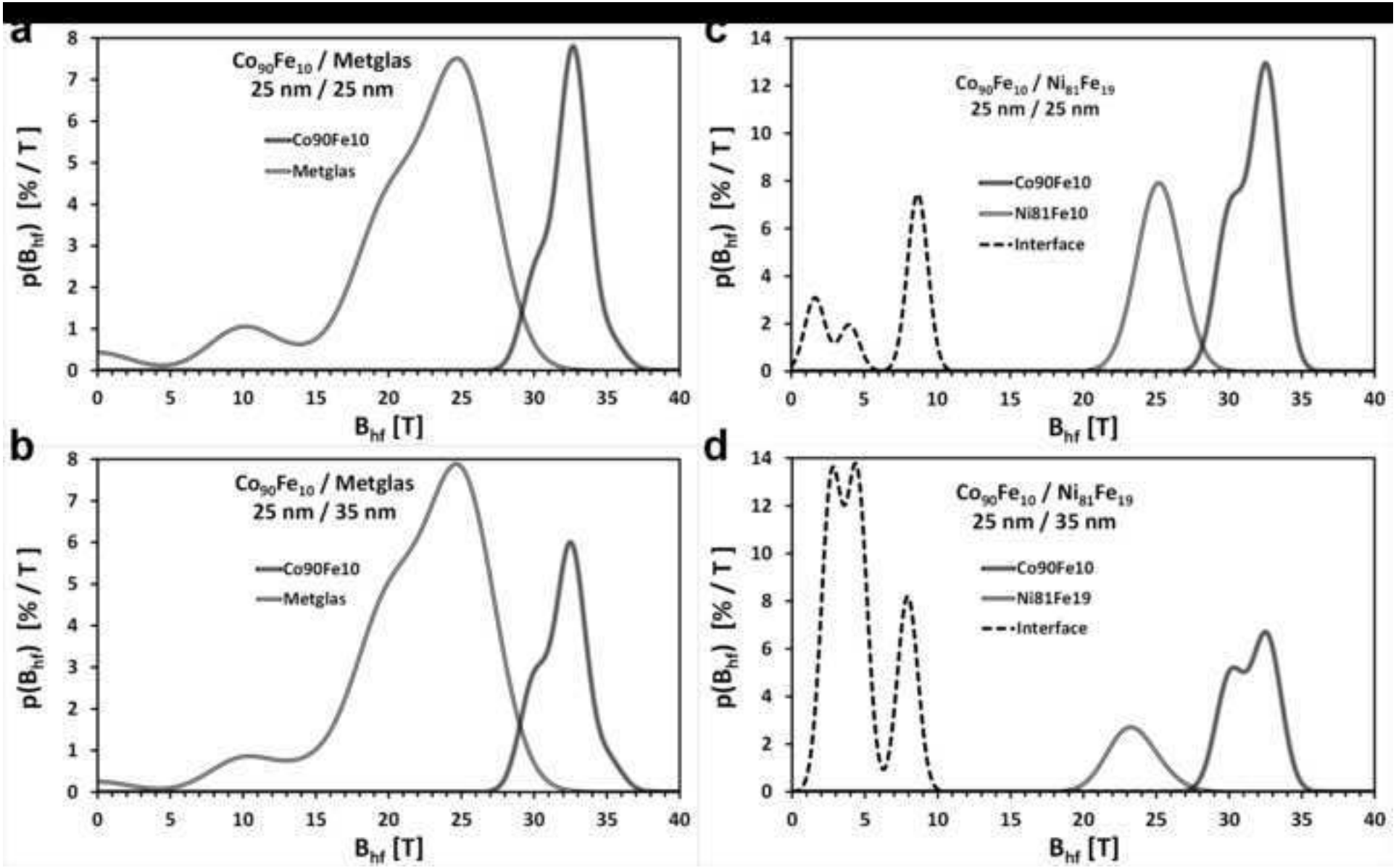

Figure
Click here to download high resolution image